Lab on a Chip

View Online
Dynamic Article Links

Cite this: DOI: 10.1039/c0lc00711k

www.rsc.org/loc

PAPER

Microfluidic fabrication of complex-shaped microfibers by liquid template-aided multiphase microflow†

Chang-Hyung Choi,[a] Hyunmin Yi,[b] Sora Hwang,[a] David A. Weitz[c] and Chang-Soo Lee*[a]

Received 20th December 2010, Accepted 16th February 2011
DOI: 10.1039/c0lc00711k

This study presents a simple microfluidic approach to the rapid fabrication of complex-shaped microfibers (*e.g.*, single hollow, double hollow, and microbelt), with highly uniform structures, based on a combination of the spontaneous formation of polymeric jet streams and *in situ* photopolymerization. Two laminar flows of a photocurable fluid and a liquid template (nonpolymerizing fluid) spontaneously form jet streams in equilibrium states in microfluidic channels because of the minimization of the interfacial energy between the two fluids. The formation of the jet streams strongly depends on the spreading coefficients and the evolution time along the downstream of the microfluidic system. Thus, the simple control of the spreading coefficients can guide microfibers into various shapes. The sizes of the core and shell of the hollow fibers can also be readily manipulated by the flow rates of the polymerizing fluid and the liquid template phase. Asymmetric hollow fibers can also be produced in different evolutionary states in the microfluidic system. The microfluidic approach shown here represents a significant step toward the easy fabrication of microfibers with readily controllable structures and geometries. We anticipate that this novel fabrication approach and the prediction method based on spreading coefficients presented in this work can be applied to produce a wide variety of functional microfibrous materials.

Introduction

Polymeric micro/nanofibers with complex shapes (*e.g.*, hollow and microbelt) have recently gained substantial attention because of their potential in many applications, such as catalysis,[1] cell culture scaffolds,[2] microreactors,[3] controlled release,[4,5] tissue engineering,[6] and adsorbent materials.[7,8]

Polymeric fibers are commonly produced by spinning or extrusion technologies, such as coelectrospinning,[9–12] hydrodynamic spinning,[13] and melting extrusion.[14,15] Among these techniques, coelectrospinning can produce hollow fibers with nanometre to submicron diameters. In a typical coelectrospinning process, a flow of polymer solution with a liquid-filled core (the liquid template) yields hollow micro/nanofibers when subjected to strong electric fields by electrohydrodynamic forces. The electrospun polymer is then rapidly solidified by evaporation. Although it provides a simple and rapid method, the coelectrospinning technique faces several challenges, including limited fiber dimensions (submicron), variability of the fiber shapes, arduous downstream processing, and the nonuniformity arising from rapid evaporation and the highly random nature of the spinning process. The hydrodynamic spinning method is another simple way to form continuous hollow fibers. Compared with coelectrospinning, this technique offers great advantages in the selection of materials that can be produced and the solidification methods available. However, it is still difficult to modulate the morphologies of the fiber structures. The extrusion process is widely used for mass production and to create complex morphologies based on designed dies. However, this method also has several disadvantages, including the limitation of the available materials (*i.e.*, thermoplastics), high production costs of complex dies, and the need for expertise in handling various parameters (*e.g.*, the temperature and the rotation rate of the screw) in the fabrication processes.

As an alternative, microfluidic systems have recently shown significant potential in the simple and rapid manufacture of highly uniform microstructures (*e.g.*, microfibers and microparticles) with *in situ* photopolymerization,[16–21] sol–gel reactions,[22] self-assembly[23] and solvent exchange.[24,25] There exist two representative microfluidic approaches to the synthesis of microfibers, which depend on the property of the wetting fluid: in one, glass capillaries promote hydrophilic wetting, and in the other, poly(dimethylsiloxane) (PDMS)-based microfluidic systems enhance the wettability of hydrophobic fluids. When glass capillary

[a]*Department of Chemical Engineering, Chungnam National University, Yuseong-gu, Deajeon, 305-764, South Korea. E-mail: rhadum @cnu.ac.kr*
[b]*Department of Chemical and Biological Engineering, Tufts University, Medford, Massachusetts, 02155, USA*
[c]*School of Engineering and Applied Sciences, Department of Physics, Harvard University, Cambridge, Massachusetts, 02138, USA*
† Electronic supplementary information (ESI) available. See DOI: 10.1039/c0lc00711k

devices use multiphase streams (inner, middle, and outer streams for the sheath flow), core–shell jets are formed and flow downstream along the capillary wall.[13,19,26] These core–shell jets are then converted into hollow microfibers upon exposure to UV radiation ("on the fly" continuous generation). However, the glass capillary method also has limitations: poor reproducibility, complex and time-consuming procedures, and the need for great care and expertise in the fabrication procedures.

Conversely, PDMS-based microfluidic systems offer several advantages arising from the inherent nature of the soft lithography, including high reproducibility, bio/chemical compatibility, low production costs, and fast prototyping.[27] Moreover, they provide various injection configurations for multiphase flow-through, precisely designed microchannels, with high scalability. However, PDMS microfluidic systems suffer from a serious drawback, in that PDMS can be swollen in organic solvents. The surface modification of PDMS with solvent-resistant materials (*e.g.*, inorganic or hybrid materials) significantly prevents its mechanical deformation, and permits harsh solvent-laden reactions to be readily performed.[28,29]

In this report, we present a simple microfluidic approach, based on the spontaneous formation of jet streams, to the rapid fabrication of various complex-shaped microfibers: single- and double-hollow microfibers and microbelts. Unlike other microfluidic approaches to the formation of core–shell hollow fibers, our proposed microfluidic method uses the basic concept of minimizing the interfacial free energy. Two dispersed fluids, the polymerizing fluid and the liquid template stream, are used together with an outer immiscible fluid, such as a hydrophobic oil phase. Under certain jetting conditions, the fluids can evolve into core–shells or more complex shapes. First, the multiphase laminar flows generate a stable formation of the core–shell jet stream and show the evolution of the multiphase (the nonequilibrium state) in different stream regions (*i.e.*, downstream from the cross-junction). The formation of core–shell or laminated jet streams in the equilibrium state is attributed to the minimization of the interfacial free energies among the three phases (liquid template, polymerizing fluid, and continuous fluid). The combination of the stable formation of the multiphase jet stream with photopolymerization successfully produces continuous hollow microfibers or microbelts in the microfluidic system. Asymmetric hollow fibers can also be produced in different evolution states in a straightforward manner.

Experimental

Materials

Poly(ethylene glycol) diacrylate (PEG-DA, $M_n = 575$), *n*-hexadecane, and 2-hydroxy-2-methylpropiophenone as the photoinitiator (PI) were purchased from Sigma-Aldrich (St Louis, MO, USA). SU-8 photoresist and developer solution was purchased from Microchem (Newton, MA, USA). PDMS was obtained from Dow Corning (MI, USA).

Fabrication of microfluidic devices

PDMS replica containing the flow-focusing geometry was generated by using a standard procedure using soft lithography.[30] The PDMS replica was exposed to oxygen plasma for 30 s, and bonded to a PDMS spin-coated glass slide. The dimensions of the microfluidic device were 50 μm × 100 μm (width × height) for the injection lines and 200 μm × 100 μm (width × height) for the jet formation area over the cross-junction.

Fabrication of microfibers

A schematic diagram of the fabrication of the microfibers is shown in Fig. 1A. The details of the microfluidic procedures used in this work are as follows. Two hydrophilic oligomeric phases (*e.g.*, 100% PEG-DA and 50% PEG-DA with PI) and a hydrophobic oil phase (*e.g.*, hexadecane with surfactant) were injected into the microfluidic device using microsyringe pumps (PHD 2000, Harvard Apparatus, MA, USA). Our method uses one (or two) liquid template stream and a polymerizing stream (the phase including the PI) together with the outer oil phase coflowing through the cross-junction, which evolves into core–shell jets or complex shapes. All the supplied reagents were combined at the cross-junction, and the jets (*e.g.*, core–shell or laminated jets) formed spontaneously. The stable jets were then exposed to 365 nm UV light (100 W UV illumination system of the microscope) to photopolymerize them to form permanent structures. UV irradiation is carried out using the objective lenses through the illumination part of the microscopy. For the fabrication of highly uniform microfibers, the jets should be fully surrounded by the outer phase during UV exposure. The polymerized microfibers were then transferred into isopropyl alcohol and washed three times with deionized water. The polymerized shell regions (50% PEG-DA with PI) then retained the permanent structure, whereas core regions (100% PEG-DA without PI) were dissolved by an organic solvent or water.

To avoid clogging problem in the microfluidic channel, we have used a microchannel with relatively high height at the

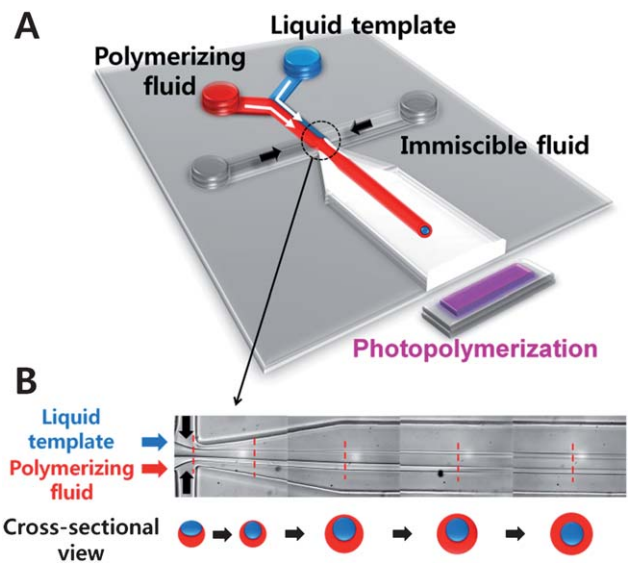

Fig. 1 Microfluidic fabrication of hollow microfibers. (A) Overall scheme of the microfluidic formation of hollow microfibers. (B) The evolution of the stratified multiphase flow; the experimental flow rate condition is $Q_C : Q_P : Q_L$ (continuous immiscible fluid : polymerizing fluid : liquid template) = 20 : 5 : 2 μL min^{-1}.

cross-junction and fabricated them under the jetting condition because multiphase jet streams are fully surrounded by the immiscible continuous phase at the cross-junction. Under the condition, we did not meet any clogging issue in the microfluidic channel while polymeric microfibers are continuously produced.

Analysis

An inverted fluorescence microscope (TE2000, Nikon, Japan) equipped with a CCD camera (Coolsnap *cf.*, Photometrics, USA) was used to examine the jet formation in the microfluidic devices. Image analysis of the microfibers was performed using ImageJ (http://rsb.info.nih.gov/ij/) and Image Pro (Media Cybernetics, MD, USA) software. The morphology of the microfibers was further characterized by scanning electron microscopy (SEM; Zeiss EVO, Carl Zeiss, Germany). The interfacial tension between the two fluids was measured using the pendant drop method (optical tensiometer; KSV Instruments, Finland). The viscosity of the PEG-DA solution was measured with a Brookfield viscometer (DV II+, MA, USA) at a rotation speed of 20 rpm.

Results and discussion

The liquid template (100% PEG-DA) and polymerizing fluid (50% PEG-DA containing 8% PI) were initially introduced into the main microchannel. The immiscible continuous fluid (*n*-hexadecane) was then loaded sequentially. These three streams coflow in a parallel formation, while fully surrounded by the immiscible hexadecane as the outer phase (Fig. 1A). Downstream, where the engulfed profile is fully developed (the equilibrium state), the multiphase streams are exposed as a jet to UV light for photopolymerization.

Sequential image analysis at different locations throughout the channel clearly showed the evolution and engulfing phenomena between the two dispersed streams (liquid template and polymerizing fluid). Specifically, under the stable condition used for the formation of the core–shell jets, we observed that the stream of polymerizing fluid (50% PEG-DA with PI) begins to engulf the liquid template stream (100% PEG-DA) near the cross-junction, where the two PEG-DA streams are positioned laterally (Fig. 1B). Downstream, the liquid template stream is fully engulfed by the stream of polymerizing fluid along the microchannel and is placed into the center of the core–shell jet (~3 mm from the T-junction). It can be seen that the shape of the interface is significantly different from that at the entrance, where the three fluids are first brought into contact side by side. Fig. 1B shows the evolution of the streams through the microfluidic channel. The final shape of the interface confirms that the formation of a hollow fiber is possible when the equilibrium at the interface of two dispersed fluids is fully established and stabilized.

The morphology can be explained by the analysis of the spreading coefficients (eqn (1); the relationships of the interfacial tensions among the three fluids) for each phase when a dispersed fluid with two liquids is brought into contact within a third immiscible liquid.[31] By combining a range of liquids, we can produce four possible two-phase particle morphologies: core–shell, occluded, acorn, and heteroaggregate.

We investigated this parameter (the spreading coefficient) to estimate the spontaneous generation of core–shell jets quantitatively, as below.

$$S_i = \gamma_{jk} - (\gamma_{ij} + \gamma_{ik}) \quad (1)$$

where γ_{jk}, γ_{ij}, and γ_{ik} are the interfacial tensions between the two phases (i, j, k). Based on this, there are three possible configurations in the equilibrium state: (i) when the conditions of (2) are satisfied, the morphology adopts a core–shell (completely engulfing) morphology, with the liquid template fluid appearing as the core within a shell of polymerizing fluid; (ii) conditions (3) correspond to stratified jetting; and (iii) conditions (4) describe separated jetting (ESI, Fig. S2†).

$$S_L < 0,\ S_P > 0,\ S_C < 0 \quad (2)$$

$$S_L < 0,\ S_P < 0,\ S_C < 0 \quad (3)$$

$$S_L < 0,\ S_P < 0,\ S_C > 0 \quad (4)$$

where S_L, S_P, and S_C are the spreading coefficients of the liquid template (100% PEG-DA), polymerizing fluid (50% PEG-DA with PI), and immiscible continuous fluid (*n*-hexadecane) streams, respectively. In this system, the measured values for these spreading coefficients (measured using the pendant drop method, Experimental section)[32] were $S_L = -2.28$, $S_P = 2.28$, and $S_C = -3.40$ mN m^{-1}, which satisfy the criteria for the formation of a core–shell structure. Thus, polymerizing fluid develops as the shell and the liquid template stream as the core. Although the surface free energy has been used to predict the morphologies of biphasic anisotropic particles (*e.g.*, peanut-like and eyeball-like particles) in electrified jet systems,[33] our results suggest that this spreading-coefficient-based estimation may also be used for core–shell jets in three-liquid-phase systems. Importantly, the conditions examined with other spreading coefficients also satisfied this theoretical proposition (ESI, Fig. S1, S2 and Tables S1, S2†), confirming the validity of the estimation method. In addition to explaining the formation of the core–shell structure with the concept of the spreading coefficient, a number of investigators have studied the factors that influence the evolution of the interface shape of the multiphase fluid components.[34,35] The most important factors influencing the interface shape are the viscosity ratio of the fluids and the length-to-diameter ratio of the microchannel. The principle of minimum viscous dissipation determines the energetically preferred interface configuration when two Newtonian fluids are forced to flow side by side through a microchannel.[36–38]

Previous studies have reported that the evolution of the core–shell structure (or the degree of interface deformation) from the initial flat interface between two fluids depends on the viscosity ratio and the residence time (the duration of fluid flow) in a microchannel.[36–38] Because the shear stress is greatest at the microchannel wall, the rate of viscous dissipation per unit length of channel will be smaller when the less viscous fluid (polymerizing fluid; 15 cP) envelopes a more viscous fluid (liquid template; 55 cP). Fig. 1B thus confirms the spontaneous formation of a core–shell structure from the flow of two fluids according to this principle.

Therefore, it can be concluded that when two fluids are introduced side by side into a microchannel, the more viscous fluid tends to become convex at the interface and the less viscous fluid tends to preferentially surround the more viscous fluid, eventually resulting in a core–shell configuration (or complete encapsulation by the less viscous fluid; the complete engulfing of the more viscous fluid by the less viscous fluid) if a sufficient evolutionary time is allowed for the flow. Therefore, our proposed approach presents a novel method for the generation of a stable core–shell structure by the spontaneous arrangement of the fluids, and we can predict the morphology using measurements of the spreading coefficients or viscosities of the multiphase fluids.

Upon UV-induced photopolymerization, these core–shell jets are solidified into permanent microfiber structures (Fig. 2). Briefly, the terminal acrylate groups of the PEG-DA monomers form reactive radicals upon photoactivation through PI, and undergo free-radical polymerization to form PEG polymers.[39] The bright-field image of Fig. 2A shows the formation of highly uniform, hollow PEG fibers with a clear interface between the core and the shell regions. The liquid template (100% PEG-DA) in the core region is not polymerized because there is no PI. We can also readily manipulate the dimensions of the core and shell regions by simply controlling the flow rate(s) of the liquid template and/or the polymerizing fluid (Fig. 2B and C). Fig. 2 clearly shows the simple changes in the core and shell thicknesses under each set of flow conditions.

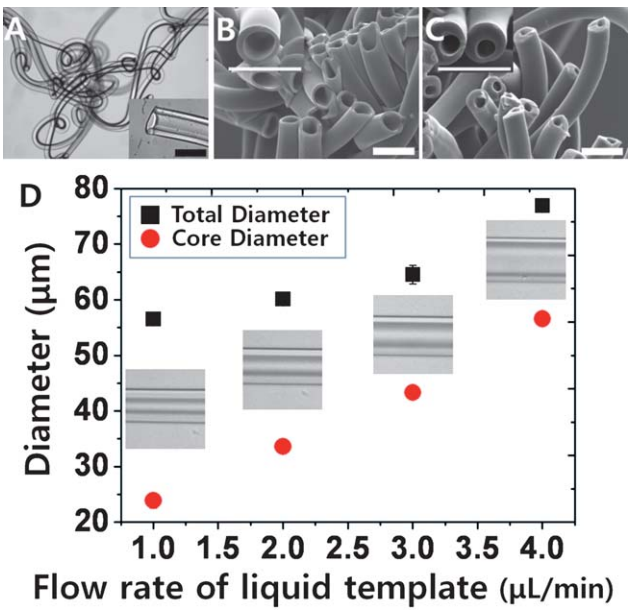

Fig. 2 The structure of hollow microfibers. (A) Bright-field image of hollow microfibers dispersed in water; these fibers were produced at $Q_C : Q_P : Q_L = 20 : 8 : 6$ μL min^{-1}. (B and C) SEM images of ruptured hollow microfibers with a single hole produced under specific flow rate conditions of $Q_C : Q_P : Q_L = 20 : 8 : 6$ and $Q_C : Q_P : Q_L = 20 : 12 : 2$ μL min^{-1}, respectively. The core size and position can be manipulated by simply controlling the flow rates of the liquid template and the polymerizing fluid. (D) The quantitative analysis of the size of the core region when the flow rate of the liquid template fluid (100% PEG-DA) is changed. Scale bars represent 50 μm.

To estimate the effects of the flow rate on the fiber morphology, the changes in the dimensions of the hollow microfibers as a function of the flow rate of the liquid template (100% PEG-DA) were investigated, while Q_C (immiscible continuous fluid) and Q_P (polymerizing fluid) were kept constant at flow rates of 20 μL min^{-1} and 4 μL min^{-1}, respectively. The increase in the flow rate of the liquid template resulted in the formation of a larger core region (Fig. 2D).[40,41] The total diameter of the hollow microfiber changed from 77 μm to 57 μm and the core diameter from 56 μm to 24 μm (Fig. 2D). The minimum size of the core region in the hollow fiber is limited by the minimum pumping capacity of the multiphase fluids during the fabrication process. Asymmetric hollow structures can also be produced if photopolymerization is performed before the cocentrical core–shell structure is fully evolved. For example, in Fig. 2C, the core–shell jets at the third stage shown in Fig. 1D are polymerized and a hollow fiber with an asymmetric core region is produced. We have sequentially fabricated different structures of hollow microfibers using four evolutionary states (ESI, Fig. S3†). Anisotropic hollow microfibers with high uniformity are promising materials in a number of biomedical applications, because specific functionalities can be tailored (*e.g.*, thicker walls for improved mechanical strength, while achieving rapid diffusion through thinner wall sections for enhanced delivery), which are highly challenging to produce with conventional methods.[42–44]

Next, we have investigated in detail the spontaneous formation of microfibers using a phase diagram to describe the different patterns observed as a function of the flow rate ratios. As shown in Fig. 3, a ternary phase diagram depicts the typical patterns of the multiphase flow: unstable jetting (I), droplet (II), jetting (III), and wetting (IV). Each axis of the diagram in Fig. 3A represents the volumetric flow rate ratios of each phase to the total flow rate (Q_T) comprising the three phases: liquid template (Q_L: 100% PEG-DA), polymerizing fluid (Q_P: 50% PEG-DA with 8% PI), and immiscible continuous fluid (Q_C: *n*-hexadecane). The total flow (Q_T) is the sum of each flow. There are unstable jetting conditions at the bottom of the phase diagram and the corresponding image is shown in Fig. 3B-I. This unstable jetting is attributed to a pressure imbalance among the fluids because the flow rates of the polymerizing fluid (Q_P) are relatively low. Specifically, the liquid template is formed into a single jet, whereas the polymerizing fluid is not injected in a stable manner. A droplet region is formed in the right bottom along the Q_P/Q_T axis (Fig. 3A and B-II). In this region, the higher flow rate of the continuous fluid (high Q_C) induces a large shear force, which causes the core–shell jet to break up into nonuniform droplets. In general, Rayleigh–Plateau instability, the phenomenon whereby a falling stream of fluid breaks up into smaller packets of equal volumes, provides enough force to form droplets from the jetting in the microfluidic system, arising from the minimization of the surface area.[45]

The mechanism and principle of the formation of uniform droplets have been developed to produce monodispersed microparticles in a microfluidic system.[16,20,21] One of the most fundamental and important issues in the formation of stable multiphase flows is to obtain a stable interface, with the desired shape, among the fluids. The position of the interface of the migrations, as the fluids flow through a microchannel, and the direction of the interface migration strongly depend on

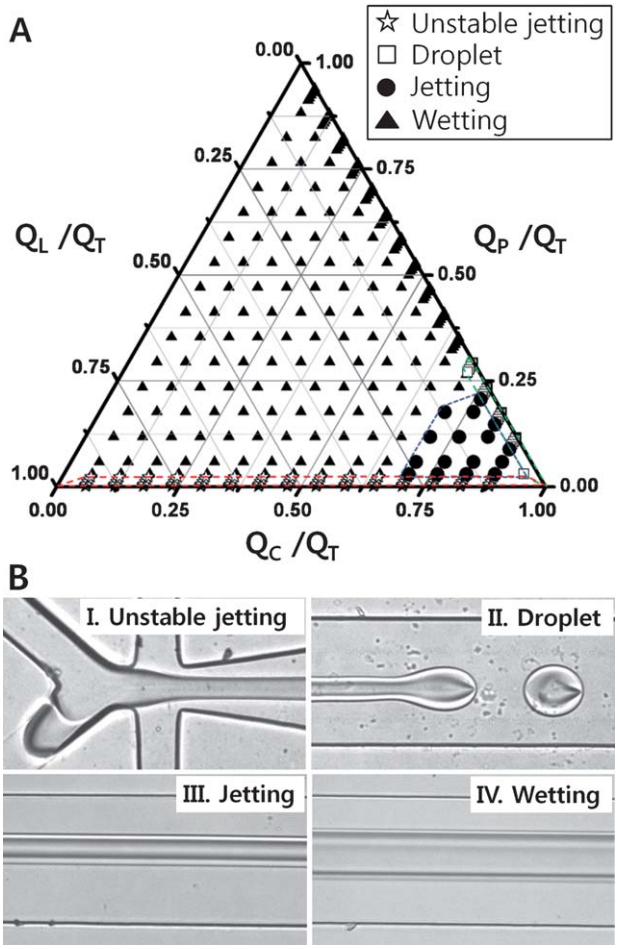

Fig. 3 The flow patterns generated in the microfluidic device. (A) Ternary-phase diagram showing four types of flow patterns (unstable jetting, droplet, jetting, and wetting) as a function of the flow rate ratios. (B) Bright-field images of each flow pattern (I–IV).

the rheological properties of the fluids involved. We found that the generation of a stable multiphase flow is possible in the right bottom region between the Q_P/Q_T and Q_L/Q_T axes (Fig. 3A). The jetting of the multiphase flow (stratified multiphase flow) is generated at high flow rates of the liquid template (Q_L) and the continuous fluid (Q_C) and a low flow rate of the polymerizing fluid (Q_P). If a liquid template is introduced as the inner fluid, a hollow microfiber with a core–shell structure can easily be obtained because the two stratified fluids (Q_L and Q_P) are fully surrounded by the immiscible continuous outer fluid (Q_C). The shape of the stable interface of the multiphase flow is confirmed (Fig. 3B-III). In the wetting region, the relatively low flow rate of the continuous fluid (Q_C) does not allow it to perfectly envelop the dispersed fluids containing the polymerizing fluid and the liquid template, so that the elongated thread of the polymerizing fluid readily sticks to the PDMS wall. Such adhesion produces serious blockages within the microchannels.

To summarize briefly, the ternary diagram provides the window on the flow parameters in the robust fabrication of hollow microfibers in microfluidic systems. Whereas this diagram is based only on the flow rates of three fluids (Q_L, Q_P, and Q_C), we envision that this diagram and the methodology presented here will provide useful information for the application of simple flow characteristics to the microfluidic fabrication of various functional materials.

Finally, we demonstrated that our microfluidic fiber fabrication method can be readily extended to produce other complex geometries (Fig. 4). First, we used microfluidic devices with three inlet streams for the introduction of two liquid template fluids (100% PEG-DA) and one polymerizing fluid (50% or 92% PEG-DA with 8% PI). Surprisingly, the introduction of two liquid template fluids generated hollow fibers with two holes upon photopolymerization (Fig. 4A).

Under the conditions used for the stable formation of a multiphase flow, the two liquid templates are positioned individually in the polymerizing fluid. Fig. 4A-I shows that the jet of the multiphase stream coflows laterally at the cross-junction. This lateral flow evolves into double core–shell jets downstream; the three black arrows indicate the polymerizing fluid streams (Fig. 4A-II). The SEM image of a ruptured microfiber clearly shows the two holes in the microfiber (Fig. 4A-III), confirming the formation of permanent double-hollow fiber structures.

Next, we investigated the effects of differences in the viscosities of the liquid template and the polymerizing fluid on the formation of the multiphase flow pattern. Three PEG-DA streams with similar compositions (liquid template of 100% PEG-DA and polymerizing fluid of 92% PEG-DA with 8% PI) coflowed to generate a stratified multiphase jetting (Fig. 4B), because the viscosity of the polymerizing fluid (92% PEG-DA with 8% PI; 50 cP) was almost the same as that of the liquid template (100% PEG-DA; 55 cP). In contrast to Fig. 4A, only three stratified flows were formed in the microchannel, although the same number and positions of fluids were introduced into the inlet ports (Fig. 4B). This indicates that the fully evolved flow pattern, in which the parallel ternary streams are fully surrounded by the outer phase, is attributable to the difference in the viscosities of the two fluids. The interfacial energy between the two fluids is also negligible, and cannot induce a fluid with low viscosity to engulf a highly viscous fluid, as is shown in Fig. 4A. As in the core–shell jet case (Fig. 1), we also used the spreading coefficient S to quantitatively estimate the flow pattern observed under this

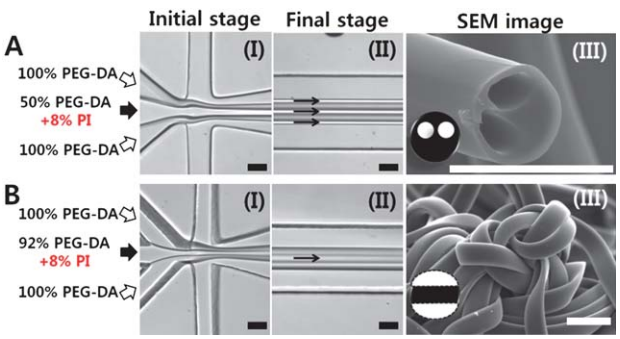

Fig. 4 Fabrication of complex-shaped microfibers. (A) Hollow microfibers with two core regions. Polymerizing fluid (50% PEG-DA with 8% PI) and liquid template (100% PEG-DA) are introduced. The ratio of the three flow rates is $Q_C : Q_P : Q_L = 20 : 12 : 2$ μL min^{-1}. (B) The generation of thin microbelts. Polymerizing fluid (92% PEG-DA with 8% PI) and liquid template (100% PEG-DA) are introduced. Scale bars represent 50 μm.

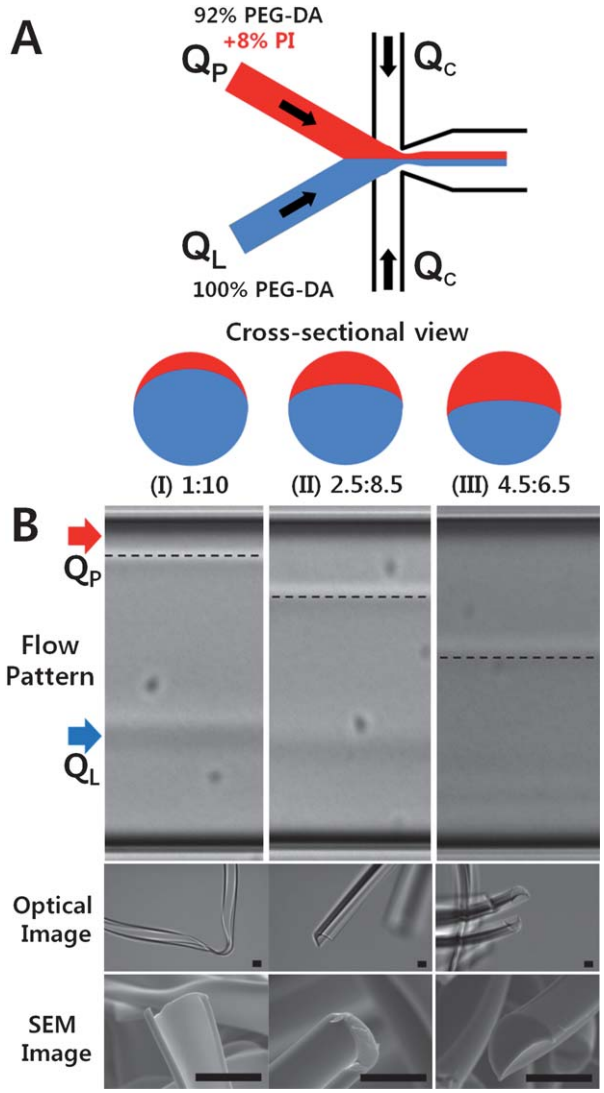

Fig. 5 Fabrication of microfibers with different cross-sections. (A) Schematic diagram of the microfluidic formation of shape-controlled microfibers and illustrations of the estimated cross-sectional shapes. The shapes are modulated by the ratios of the volumetric flow rates; the ratios of the two fluids ($Q_P : Q_L$) were 1 : 10, 2.5 : 8.5, and 4.5 : 6.5, respectively, whereas the flow rate of the continuous fluid (Q_C) was fixed (24 μL min^{-1}). (B) The synthesis of microfibers with different cross-sections using the continuous introduction of two fluids, the polymerizing fluid (92% PEG-DA with 8% PI) and the liquid template (100% PEG-DA). Bright-field images and SEM images clearly show the production of microfibers with different cross-sectional shapes. Scale bars represent 50 μm.

condition. The spreading coefficients of the three streams (liquid template, polymerizing fluid, and continuous fluid) were individually calculated to be S_L −3.66, S_P −0.18, and S_C −5.86 mN m^{-1}, which satisfy the conditions for stratified jetting flow among the fluids. This estimation is consistent with the experimental results shown in Fig. 1 (engulfing), as well as those in Fig. 4 (stratified jetting). This theoretical estimation should be a useful criterion in establishing the prototype design principles for the formation of complex-shaped microfibers. The SEM image clearly shows the detailed structure of the microbelt (belt-like structure), with a flat top and rounded sides (Fig. 4B).

Importantly, the results shown in Fig. 4 confirm that we can further manipulate the shapes of microfibers by changing the configuration of the streams by simply controlling the viscosity ratio of the liquid template and the polymerizing fluid. We can further extend this technique to tailor microfibers with different cross-sectional shapes by the simple modulation of the volumetric ratio of the two fluids (100% PEG-DA as the liquid template and a polymerizing fluid of PEG-DA) under the conditions of stratified jetting (Fig. 5A). The bottom illustration in Fig. 5A shows the cross-sectional shapes estimated when the fluids are introduced in different ratios (I–III; $Q_P : Q_L = 1 : 10$, 2.5 : 8.5, and 4.5 : 6.5, respectively). We investigated the shapes of the microfibers synthesized with various ratios of the two fluids. Two PEG-DA streams, one with PI and the other without PI, coflowed to produce stratified jetting with relatively different proportions of the polymerizing fluid (Fig. 5B). After UV-induced polymerization, optical and SEM images provide detailed information on the microfiber structures. An increase in the proportion of polymerizing fluid (92% PEG-DA with PI) produced thicker hemispherical microfibers. There is a curved profile of the cross-section along the longitude in the microfibers because of the wetting curvature between the liquid template and the polymerizing fluid (Fig. 5B).

Therefore, our microfluidic approach can be used to produce a wide range of microfiber geometries. The formation of various morphologies can be estimated from the spreading coefficients or the minimum viscous dissipation. Although we have only examined PEG-DA in this study, we anticipate that our approach can be applied to other chemicals (*e.g.*, curable polymers, monomers, and inorganic materials) to produce a broad range of functionalities and properties. Moreover, thermodynamic manipulation by simply controlling the rheological characteristics of viscosity and flow rate will be useful in the fabrication of microfibers with complex microstructures.

Conclusions

In this paper, we have presented a simple microfluidic method based on the spontaneous formation of a multiphase flow, such as an engulfing flow or a stratified multiphase flow, for the fabrication of complex-shaped microfibers. This microfluidic fabrication allows continuous *in situ* production, high reproducibility, easy integration of complex designs, and complex processes. The combination of the spontaneous evolution of multiphase flow patterns with photopolymerization is a valuable alternative technique for the synthesis of novel microfibers with highly uniform dimensions. An asymmetric hollow microfiber, with no concentric core, can also be produced at the different evolution state. Our strategy for the fabrication of microfibers could be readily applied in conjugated microfibers, multilayer flat fibers or films, multilayer blown fibers, hollow cables and wires, sandwiched foam composites, encapsulation of active agents, cell culture scaffolds, catalysts support, affinity membranes, hierarchical filter materials, or protective clothing because of their large surface area and pore connectivity. To expand our proposed approach successfully to other applications, it will be important to investigate a wide range of processing variables, the rheological properties of the individual fluids, and the designs of microfluidic systems. Moreover, the theoretical estimates based

on spreading coefficients are a critical factor if the design is to be used for the configuration of microfibers. Our proposed microfluidic method can be readily extended to other chemical reaction systems (*e.g.*, solvent exchange, sol–gel reactions, or interfacial polymerizations) for the development of novel functional microfibers with controlled compositions and microstructures.

Acknowledgements

This research was supported by the National Space Laboratory (NSL) program through the National Research Foundation of Korea, funded by the Ministry of Education, Science and Technology (20100026155), and the Converging Research Center Program, through the Ministry of Education, Science and Technology of Korea (2010K001055).

References

1 Z. Wen, Q. Wang and J. Li, *Adv. Funct. Mater.*, 2008, **18**, 959–964.
2 J.-H. Jung, C.-H. Choi, S. Chung, Y.-M. Chung and C.-S. Lee, *Lab Chip*, 2009, **9**, 2596–2602.
3 S. Chen, E. Kim, M. L. Shuler and D. B. Wilson, *Biotechnol. Prog.*, 1998, **14**, 667–671.
4 H. K. Tilakaratne, S. K. Hunter, M. E. Andracki, J. A. Benda and V. G. Rodgers, *Biomaterials*, 2007, **28**, 89–98.
5 J. M. Schnur, *Science*, 1993, **262**, 1669–1676.
6 A. Khademhosseini, R. Langer, J. Borenstein and J. P. Vacanti, *Proc. Natl. Acad. Sci. U. S. A.*, 2006, **103**, 2480–2487.
7 R. P. Lively, R. R. Chance, B. T. Kelley, H. W. Deckman, J. H. Drese, C. W. Jones and W. J. Koros, *Ind. Eng. Chem. Res.*, 2009, **48**, 7314–7324.
8 Y. Zhang and A. Reller, *Chem. Commun.*, 2002, 606–607.
9 I. G. Loscertales, A. Barrero, M. Marquez, R. Spretz, R. Velarde-Ortiz and G. Larsen, *J. Am. Chem. Soc.*, 2004, **126**, 5376–5377.
10 D. Li and Y. Xia, *Adv. Mater.*, 2004, **16**, 1151–1170.
11 Y. Hong, X. Chen, X. Jing, H. Fan, Z. Gu and X. Zhang, *Adv. Funct. Mater.*, 2010, **20**, 1503–1510.
12 Y. Dror, W. Salalha, R. Avrahami, E. Zussman, A. L. Yarin, R. Dersch, A. Greiner and J. H. Wendorff, *Small*, 2007, **3**, 1064–1073.
13 M. Hu, R. Deng, K. M. Schumacher, M. Kurisawa, H. Ye, K. Purnamawati and J. Y. Ying, *Biomaterials*, 2010, **31**, 863–869.
14 T. He, M. H. V. Mulder, H. Strathmann and M. Wessling, *J. Membr. Sci.*, 2002, **207**, 143–156.
15 L. Jiang, T.-S. Chung, D. F. Li, C. Cao and S. Kulprathipanja, *J. Membr. Sci.*, 2004, **240**, 91–103.
16 Z. Nie, S. Xu, M. Seo, P. C. Lewis and E. Kumacheva, *J. Am. Chem. Soc.*, 2005, **127**, 8058–8063.
17 T. Nisisako and T. Torii, *Adv. Mater.*, 2007, **19**, 1489–1493.
18 D. Dendukuri, D. C. Pregibon, J. Collins, T. A. Hatton and P. S. Doyle, *Nat. Mater.*, 2006, **5**, 365–369.
19 W. Jeong, J. Kim, S. Kim, S. Lee, G. Mensing and D. J. Beebe, *Lab Chip*, 2004, **4**, 576–580.
20 A. S. Utada, E. Lorenceau, D. R. Link, P. D. Kaplan, H. A. Stone and D. A. Weitz, *Science*, 2005, **308**, 537–541.
21 C.-H. Choi, J.-H. Jung, D.-W. Kim, Y.-M. Chung and C.-S. Lee, *Lab Chip*, 2008, **8**, 1544–1551.
22 I. Lee, Y. Yoo, Z. Cheng and H.-K. Jeong, *Adv. Funct. Mater.*, 2008, **18**, 4014–4021.
23 P. S. Dittrich, M. Heule, P. Renaud and A. Manz, *Lab Chip*, 2006, **6**, 488–493.
24 W. Lan, S. Li, Y. Lu, J. Xu and G. Luo, *Lab Chip*, 2009, **9**, 3282–3288.
25 C. M. Hwang, A. Khademhosseini, Y. Park, K. Sun and S. H. Lee, *Langmuir*, 2008, **24**, 6845–6851.
26 K. H. Lee, S. J. Shin, Y. Park and S.-H. Lee, *Small*, 2009, **5**, 1264–1268.
27 D. C. Duffy, J. C. McDonald, O. J. A. Schueller and G. M. Whitesides, *Anal. Chem.*, 1998, **70**, 4974–4984.
28 B.-Y. Kim, L.-Y. Hong, Y.-M. Chung, D.-P. Kim and C.-S. Lee, *Adv. Funct. Mater.*, 2009, **19**, 3796–3803.
29 A. R. Abate, D. Lee, T. Do, C. Holtze and D. A. Weitz, *Lab Chip*, 2008, **8**, 516–518.
30 Y. Xia and G. M. Whitesides, *Angew. Chem., Int. Ed.*, 1998, **37**, 550–575.
31 S. Torza and S. G. Mason, *J. Colloid Interface Sci.*, 1970, **33**, 67–83.
32 B. Song and J. Springer, *J. Colloid Interface Sci.*, 1996, **184**, 77–91.
33 K.-H. Roh, D. C. Martin and J. Lahann, *Nat. Mater.*, 2005, **4**, 759–763.
34 C. D. Han, *Multiphase Flow in Polymer Processing*, Academic Press, New York, 1981, p. 400.
35 H. M. A. Karagiannis, A. N. Hrymak and J. Vlachopoulos, *Polym. Eng. Sci.*, 1988, **28**, 982–988.
36 D. L. MacLean, *J. Rheol.*, 1973, **17**, 385–399.
37 J. A. E. Everage, *J. Rheol.*, 1973, **17**, 629–646.
38 B. Khomami, *J. Non-Newtonian Fluid Mech.*, 1990, **37**, 19–36.
39 D. Dendukuri, P. Panda, R. Haghgooie, J. M. Kim, T. A. Hatton and P. S. Doyle, *Macromolecules*, 2008, **41**, 8547–8556.
40 Z. Wu and N.-T. Nguyen, *Sens. Actuators, B*, 2005, **107**, 965–974.
41 N.-T. Nguyen, Y.-F. Yap and A. Sumargo, *Meas. Sci. Technol.*, 2008, **19**, 085405.
42 D. Wang, K. Li and W. K. Teo, *J. Membr. Sci.*, 2000, **178**, 13–23.
43 D. Li, T.-S. Chung and R. Wang, *J. Membr. Sci.*, 2004, **243**, 155–175.
44 S.-H. Choi, F. Tasselli, J. C. Jansen, G. Barbieri and E. Drioli, *Eur. Polym. J.*, 2010, **46**, 1713.
45 J. W. S. Rayleigh, *Proc. R. Soc. London*, 1878, **10**, 4–11.